J Solid State Electrochem (2001) 6: 55–62
DOI 10.1007/s100080100194

ORIGINAL PAPER

R. Alcántara · F.J. Fernández Madrigal · P. Lavela
C. Pérez-Vicente · J.L. Tirado

Tin oxalate as a precursor of tin dioxide and electrode materials for lithium-ion batteries

Received: 2 May 2000 / Accepted: 5 December 2000 / Published online: 16 May 2001

Abstract Tin(II) oxalate was studied as a novel precursor for active electrode materials in lithium-ion batteries. The discharge of lithium cells using tin oxalate electrodes takes place by three irreversible steps: tin reduction, forming a lithium oxalate matrix; solvent decomposition to form a passivating layer; and oxalate reduction in a two-electron process. These are followed by reversible alloying of tin with lithium, leading to a maximum discharge of 11 F/mol. Cycling of the cells showed reversible capacities higher than 600 mAh/g during the first five cycles and ca. 200 mAh/g after 50 cycles. Tin oxalate was converted to tin dioxide by thermal decomposition at 450 °C and also by a chemical method by dissolving tin oxalate powder in 33% v/v hydrogen peroxide at room temperature. The ultrafine nature of the tin dioxide powders obtained by this procedure allow their use as electrodes in lithium cells. The best capacity retention during the first five cycles was achieved for a sample heat treated to 250 °C to eliminate surface water.

Keywords Tin oxalate · Tin dioxide · Lithium-ion batteries · Step potential electrochemical spectroscopy

Introduction

Tin(IV) dioxide is widely used in commercially manufactured sensors for polluting and combustible gases such as CO [1, 2]. This and other relevant industrial applications of SnO_2, such as an opacifier for glazes and enamels, a base for pigments, an additive in glasses and in heterogeneous catalyst, etc., demand new methods of synthesis and a better control over the textural and structural properties. The solid can be prepared in the form of thin-film products as well as a powdered material by alternative routes, which include the sol-gel route [2, 3] and spray pyrolysis [4].

On the other hand, studies on tin dioxide and other tin compounds as anode materials for lithium-ion batteries have been extended quite rapidly in recent years. After the report by members of the Fuji research laboratories which demonstrated that tin-based amorphous oxides were able to deliver high specific capacities for a large number of cycles [5], several crystalline tin oxides (SnO [6], SnO_2 [7]) and salts (e.g. SnP_2O_7 [8], $SnSO_4$ [9] and Sn_2PO_4Cl [10]) have been tested as potential candidates. Thin films of tin dioxide have also been proven to have an excellent capacity retention [11, 12].

Low-temperature decomposition of organic precursors containing a chelating reagent has been reported as a good method to prepare transition metal oxides for use as positive electrodes in lithium batteries [13, 14, 15]. The precursor route allows the synthesis of nanocrystals with a good control over composition and structure. Possible advantages may arise from the use of oxalate precursors as a result of the low cost of the reagents and the ultrafine nature of the particles obtained. This has prompted us to examine the possibilities of tin(II) oxalate with a twofold objective: an active material for battery electrodes within the lithium-ion technology, and a precursor for tin dioxide by using thermal and chemical methods.

Experimental

Commercial tin(II) oxalate (Strem) was used as received as an active electrode material and as an organic salt precursor in the preparation of the tin oxides. The thermal decomposition of tin(II) oxalate was monitored using thermogravimetric analysis (TGA) with a Cahn 2000 electrobalance.

The chemical method to convert the precursor into tin dioxide consisted of dissolving tin oxalate powder in 33% v/v hydrogen peroxide at room temperature. The clear solution was then smoothly heated with stirring until boiling. Parallel to water evaporation, a white colloidal product precipitates. The continuous

R. Alcántara · F.J.F. Madrigal · P. Lavela · C. Pérez-Vicente
J.L. Tirado (✉)
Laboratorio de Química Inorgánica,
Universidad de Córdoba, Campus de Rabanales,
Edificio C3, planta 1, 14071 Córdoba, Spain
E-mail: iq1ticoj@uco.es

heating provokes water evaporation of the colloidal solution until a white solid product precipitates. The dry powder (henceforth referred to as pristine sample) was collected, ground and stored in an oven at 60 °C. The thermal behaviour of the solid product was followed by TGA and evolved gas analysis (EGA) was carried out with a quartz reactor coupled with a quadrupole mass spectrometer (model VG sensorlab). The gas carrier used was nitrogen.

X-ray diffraction (XRD) patterns were obtained with a Siemens D5000 apparatus working with Cu Kα radiation and a graphite monochromator. Fourier transform Raman spectra were obtained with a Perkin-Elmer 2000 R system working with a 10,000 cm^{-1} neodymium:yttrium aluminum garnet (Nd:YAG) laser radiation source. Fourier transform infrared (FTIR) spectra were obtained in the 400–4000 cm^{-1} region using a Bomem HB-100 spectrometer. Transmission electron microscopy (TEM) analyses were carried out on a JEOL-200CX instrument.

The electrochemical behaviour of the tin oxalate precursor and the tin dioxide samples derived by thermal and chemical treatments was tested by step potential electrochemical spectroscopy (SPES). A multichannel system (MacPile) was used, working under galvanostatic and potentiostatic conditions. Two-electrode Swagelok-type $Li/LiPF_6$ (EC:DMC = 1:1)/test-electrode cells were prepared as follows. The test electrodes were prepared as 7 mm diameter pellets by pressing at 200 MPa a mixture of 60% of sample (ca. 3 mg) and 10% of polytetrafluoroethylene (PTFE) binder and 30% carbon black (Strem 4N) to improve the mechanical and electronic conduction properties. The lithium electrodes consisted of a clean 7 mm diameter lithium metal disc. The electrolyte solution was supported by porous glass-paper discs. All cell manipulations were carried out inside the glove box (Braun) under an argon atmosphere (water content < 2 ppm).

Results and discussion

Prior to its chemical modification, the phase purity of commercial tin(II) oxalate was checked by recording the XRD patterns to see that they properly matched the JCPDS file (no. 17-0743). The FTIR spectrum (Fig. 1a) showed the characteristic bands: two doublets at 1606–1674 and 1299–1336 cm^{-1} ascribable to asymmetric and symmetric C-O stretching, respectively, a narrow and intense signal at 788 cm^{-1} due to O-C = O deformation, and two signals at 480 and 428 cm^{-1} ascribable to ring deformations and Sn-O stretching [16]. Furthermore, TGA data of tin(II) oxalate recorded in a static air atmosphere showed a single weight loss in a narrow range of temperature at around 350 °C, whose magnitude (ca. 30%) agrees fairly well with the following reaction:

$$SnC_2O_4 + Q \rightarrow SnO_2 + 2CO \quad (1)$$

XRD patterns of the thermally decomposed products obtained at 450 °C for different annealing periods are basically characteristic of tin dioxide with a rutile-type structure (JCPDS file no. 41-1445). Irrespective of annealing time, the FTIR spectra (Fig. 1b) show two symmetry allowed Sn-O stretching bands of rutile-type SnO_2 (D_{4h}, E_u *xy*-plane and A_{2u} *z*-axis modes) located at 618 and 477 cm^{-1}, respectively [17, 18]. Two additional effects are also observed which were ascribed by Opara Krasovec et al. [17] as due to the relaxation of the selection rules of the crystal by the A_{1g} Raman (symmetric Sn-O stretch) and the B_{1u} (Sn-O-Sn bending) silent modes at 670 and 530 cm^{-1}, respectively. The TEM observations of the ex-oxalate SnO_2 particles obtained by thermal treatment (Fig. 2) reveal that the external size and shape of the initial oxalate particles is preserved after thermal treatment. However, the texture of the bulk particles is characterized by domains of ca. 70 nm size which define a macroporous system.

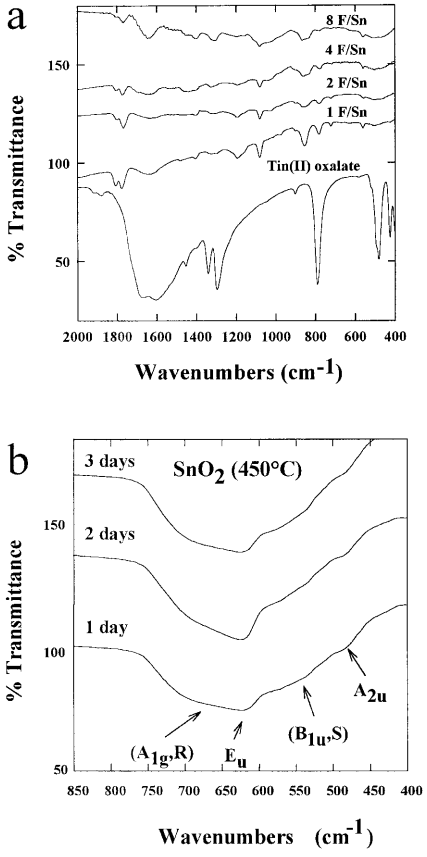

Fig. 1 FTIR spectra of **a** tin(II) oxalate and oxalate-based electrodes after discharge to 1, 2, 4 and 8 F/Sn, and **b** SnO_2 prepared by thermal decomposition of tin(II) oxalate at 450 °C in an air atmosphere and annealed for different periods

The electrochemical behaviour of commercial tin oxalate was tested by directly using the compound in the positive electrode of lithium anode cells. Three different experiments were performed on these cells: (1) step potential electrochemical spectroscopy (SPES) at 10 mV/0.1 h rate, (2) galvanostatic intermittent titration (GITT) with 15 min current pulses followed by 30 min voltage relaxation periods, and (3) constant current galvanostatic cycling at C/2 rate (2 F/mol in 1 h). The SPES curve in Fig. 3 a reveals a broad reduction band with a complex shape during the first discharge to 0 V. The reactions leading to these effects cannot be ascribed exclusively to tin reduction followed by alloying processes as found in other tin salts, as the maximum capacity obtained was close to 11 F/mol of SnC_2O_4. Nevertheless, the reversible capacity found during the first cycles (Fig. 3b) agrees well with the alloying of

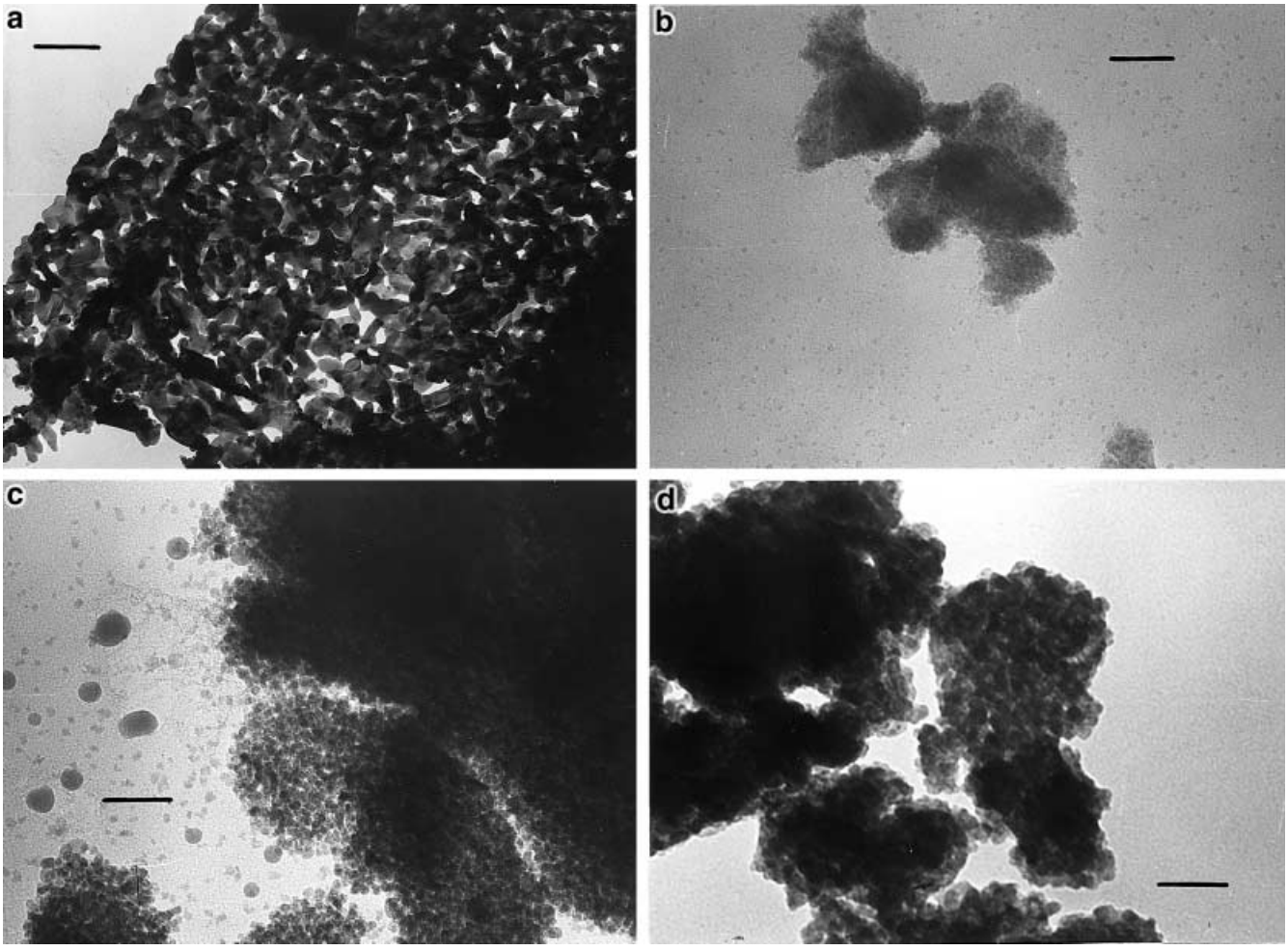

Fig. 2 TEM of ex-oxalate SnO_2 samples: **a** prepared by thermal decomposition at 450 °C, **b** pristine chemically prepared sample, **c** chemically prepared sample heat treated at 250 °C, and **d** chemically prepared sample heat treated at 450 °C. Magnification for **a**: *bar* = 150 nm; **b**–**d**: *bar* = 30 nm

lithium up to $Li_{22}Sn_5$ composition (4.4 F/mol) The additional reactions contributing to the irreversible capacity were examined as follows.

The reaction:

$$SnC_2O_4 + 2Li^+ + 2e^- \rightarrow Sn + Li_2C_2O_4 \quad (2)$$

is expected during the first steps of discharge. An indirect proof of Eq. 2 was obtained by XRD data, which show the loss of the SnC_2O_4 reflections between 0 and 2 F/Sn. The XRD patterns revealed the lack of long-range order of the products, with no direct evidence of crystalline oxalate or other side products at 2 F/Sn. It should be noted that the voltage observed for Sn(II) reduction agrees with previous reports on the reaction with lithium of different Sn(II) oxy salts [8, 9, 10]. Moreover, the first voltage step in the plot of cell potential versus F/Sn (Fig. 3) involves a consumption of 2 Li per mole of active material. This value agrees well with the extent of Eq. 2.

The formation of a SEI layer according to:

$$EC/DMC + Li^+ + e^- \rightarrow SEI(Li_2CO_3/LiO_2COR) \quad (3)$$

was also checked. In contrast to the fixed stoichiometry of Eq. 2, Eq. 3 involves electrolyte decomposition in a variable extension in the surface of the electrode, leading to inorganic and organic carbonates until a passivating film is formed. In Fig. 3, these processes take place between 1.2 and 0.7 V. A similar process has been detected prior to the Sn^{2+}/Sn reduction in SnO electrodes below 1.2 V [19]. However, it should be noted that SnO reduction reported by these authors occurs below 0.9 V.

Besides, Eq. 3 was monitored by the FTIR spectra of tin(II) oxalate-based electrodes, after careful rinsing with dry hexane, in which carbonate/alkyl carboxylate groups were identified. Figure 1a compares the FTIR spectra of the oxalate precursor and the discharged products up to 8 F/Sn. The transmission band of the oxalate group remained detectable for a depth of discharge of 4 F/Sn, which shows its persistence during the electrochemical Eqs. 2 and 3. Nevertheless, the spectra undergo significant changes affecting both the shape of the bands corresponding to CO vibrations and the occurrence of new peaks. Thus, the doublets at 1606–1674 and 1299–1336 cm^{-1} coalesce into two broadened signals

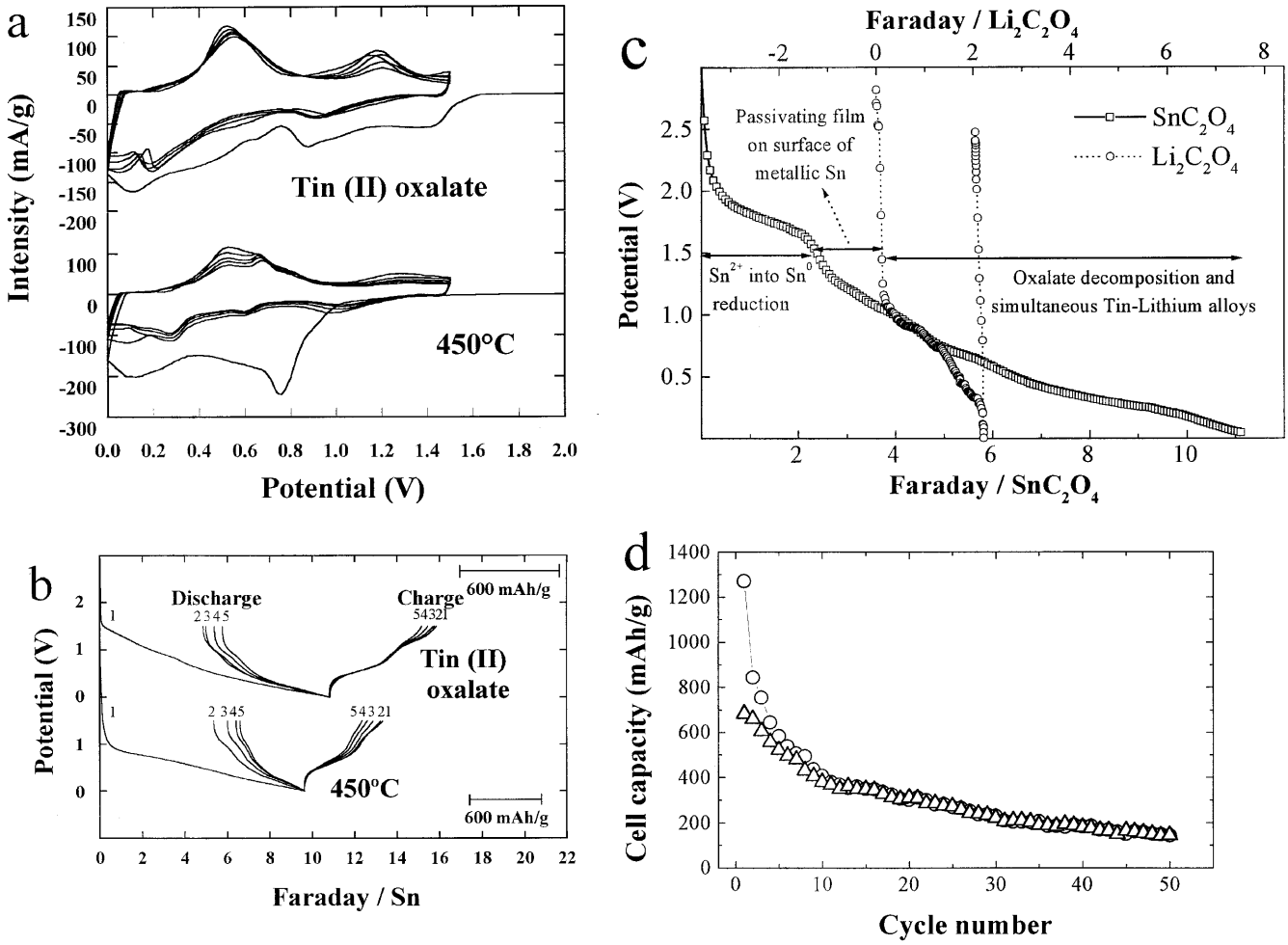

Fig. 3 **a** Current intensity vs. potential curves and **b** potential vs. composition curves obtained by SPES of lithium cells using tin(II) oxalate and SnO_2 (obtained by thermal decomposition of tin oxalate at 450 °C) as electrode materials. **c** GITT curves of lithium cells using $Li_2C_2O_4$ and SnC_2O_4 electrode materials. **d** Galvanostatic cycling behaviour of SnC_2O_4 cells

centred at ca. 1650 and 1350 cm^{-1}, respectively. These changes are probably indicating the conversion to lithium oxalate, although a possible overlap with those bands belonging to additional products generated in reaction 3 cannot be discarded. In addition, several signals are ascribable to CO_3^{2-} and $ROCO_2Li$ groups, in good agreement with previous results obtained by Aurbach et al. [20]. Thus, two broadened signals at ca. 860 and 1085 cm^{-1} in the product from the 1 F/Sn discharged electrode may correspond to CO_3^{2-} vibrations. The occurrence of these signals even at early stages of discharge (1 F/Sn) may indicate a certain degree of overlap between Eqs. 2 and 3. Some additional bands at ca. 1196 and 1766 cm^{-1} are attributable to EC residua [20].

A third process that may contribute to the initial irreversible capacity is the reduction of the lithium oxalate produced in Eq. 1. Several reactions leading to a decrease in the oxidation state of carbon could be involved. Although at present we have no direct evidence of the reaction products, a simple two-electron reduction could be suggested, according to:

$$Li_2C_2O_4 + 2Li^+ + 2e^- \rightarrow 2Li_2O + 2CO \quad (4)$$

In order to demonstrate the contribution of oxalate decomposition, GITT data were obtained and compared for lithium cells using alternatively $Li_2C_2O_4$ and SnC_2O_4 samples in the positive electrode (Fig. 3c). As one can see, the complex profile at ca. 1 V vs. Li for the discharge of the $Li_2C_2O_4$ cell leads to a consumption of 2 F/mol, which agrees well with the stoichiometry in Eq. 4. Moreover, the potential interval in which the discharge develops is comparable with a third region in the SnC_2O_4 cell. Also, the irreversible nature of the process is shown by the lack of charging ability of the $Li_2C_2O_4$ cell shown in Fig. 3c.

Finally, the description of the SPES and galvanostatic cycling curves below 0.7 V (Fig. 3d) agrees well with the reversible formation of $Li_{22}Sn_5$ alloy. The passivating residua prevent aggregation of the tin alloy particles, which agrees well with a good capacity retention during initial cycling (Fig. 3). However, it is worth noting that the cycling behaviour of tin(II) oxalate is good, particularly for the first few cycles (Fig. 3). In fact,

a capacity higher than 600 mAh/g was retained during the first five cycles. On increasing the cycle number, a significant decrease in reversible capacity is found. Still, the values after 50 cycles (ca. 200 mAh/g) are better than those found in other alternative materials for lithium-ion technology, such as petroleum cokes.

On the other hand, the tin dioxide sample obtained by the thermal decomposition of SnC_2O_4 and annealed for 2 days was tested in lithium cells and the results are also shown in Fig. 3 for comparative purposes. The first reduction of ex-oxalate tin dioxide shows only two signals. Such behaviour has been extensively described in previous works (e.g. [6, 7]). The sharp peak at ca. 0.8 V is due to lithium oxide formation, while the lower voltage wave corresponds to the formation of Li-Sn alloys. Further discharges are quite different with respect to that described above. Moreover, the observed reproducibility of the curve shape, at least up to cycle five, is indicative of homogeneity in the redox reaction probably caused by good dispersion effects originating from redox irreversible products on the tin alloy particles.

The chemical method used to convert the precursor into tin dioxide by treating tin(II) oxalate with hydrogen peroxide led to an additional set of powder samples. The XRD patterns were recorded for pristine materials and for several products obtained by heating the former solid in air at different temperatures for 12 h. The XRD patterns are displayed in Fig. 4. The as-prepared oxide shows several broadened diffraction maxima which are coincident with the more intense reflection of the SnO_2 rutile-type structure and are indicative of a particularly low size of the coherently diffracting domains. Besides, some authors have pointed out the possibility that SnO_2 particles with low particle size may show a tendency to become orthorhombic, thus contributing to the broadening of the XRD bands [21].

A significant decrease in line broadening with the heating temperature is clearly observed, which implies an expected augmentation in the size of the particle domains. TEM observation of the particles reveals the presence of irregularly shaped agglomerates of ultrafine particles in the as-prepared product. The mean size takes a value of ca. 3 nm and increases to 5, 7, 12 and 16 nm on increasing the annealing temperature to 250, 450, 650 and 800 °C, respectively.

The ultrafine nature of the as-prepared chemical sample discussed above agrees well with the Raman spectroscopy data. Several authors have examined in detail the effects of particle size on the Raman spectra of tin dioxide. In this way, Abello et al. [18] established a direct relationship between the textural properties and the relative intensity of surface and volume modes. In an attempt to evaluate the contribution of the surface modes to the spectrum of the as-prepared chemical sample shown in Fig. 5, the computer program

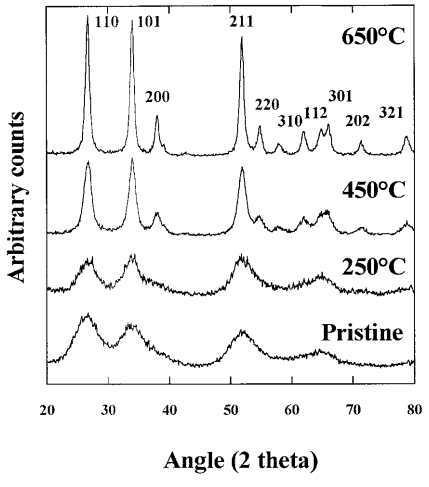

Fig. 4 XRD patterns of pristine chemically decomposed tin oxalate and heat-treated products

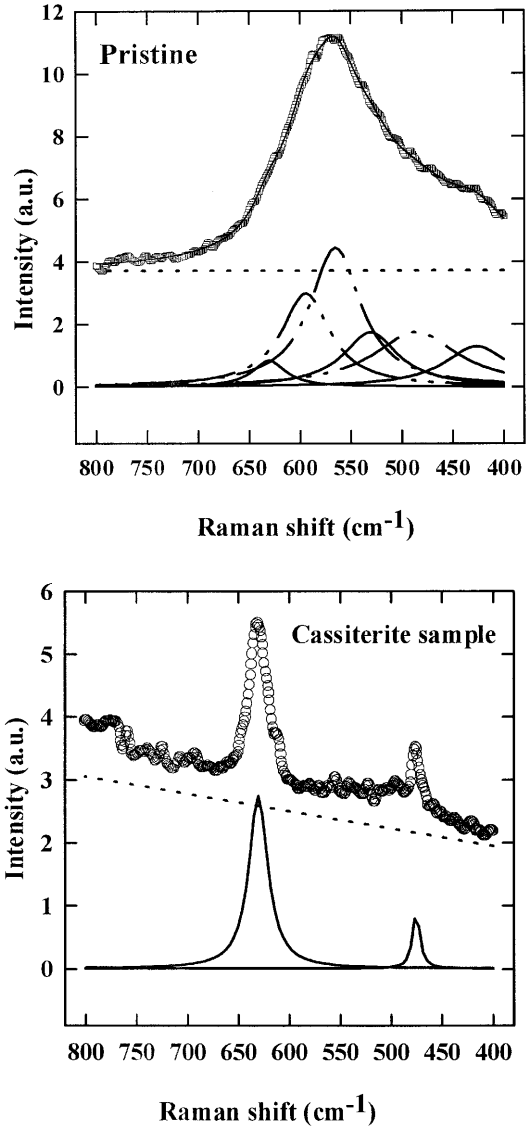

Fig. 5 FT-Raman spectra of pristine chemically decomposed tin oxalate (*upper*) and commercial cassiterite (*lower*)

PEAKFIT was applied. Six bands were found to describe accurately the spectrum. The two most intense bands occur at 565 and 594 cm^{-1} and can be unambiguously ascribed to surface modes [17], while the bands at 630 and 485 are ascribable to the Raman-allowed A_{1g} and E_g volume modes, respectively. In contrast, for a crystalline cassiterite sample also shown in Fig. 5, the volume modes dominate the spectrum, as also found in the sintered oxide by other authors [17, 18, 19].

On the other hand, the FTIR data of the samples prepared by the H_2O_2 route (Fig. 6) shows some common effects with those of the thermal samples (Fig. 1). In addition, the presence of OH groups and surface and/or occluded water is evidenced by the O-H stretch band at ca. 3400 cm^{-1} and the HOH deformation at 1630 cm^{-1}. These bands are lost almost completely between 450 and 650 °C (Fig. 6). The fact that water content is released up to 650 °C was confirmed by the EGA and TGA experiments (Fig. 7). According to these results, water is released in two well-defined steps below and above 200 °C. The second, broader wave extends up to 600 °C. Below 200 °C, surface and occluded water is probably directly responsible for the weight loss in these materials. Above this temperature, structural water is released.

The effect of textural and compositional evolution of the samples is reflected in the electrochemical behaviour. The potentiostatic cycling showed a reproducible charge and discharge process for the pristine chemically prepared material and the heat-treated products (Fig. 8). A clear evolution of the voltammograms is particularly seen when comparing the first cell discharge branches, in which a peak at ca. 0.75 V is developed on increasing temperature. This peak can be ascribed, as in the thermally obtained sample (Fig. 3), to lithium oxide/metallic tin formation from the dehydrated tin dioxide. In pristine and 250 °C heat-treated samples the process is more complex and less defined, probably due to the contribution of the small particle size and side reactions with surface and/or structural water.

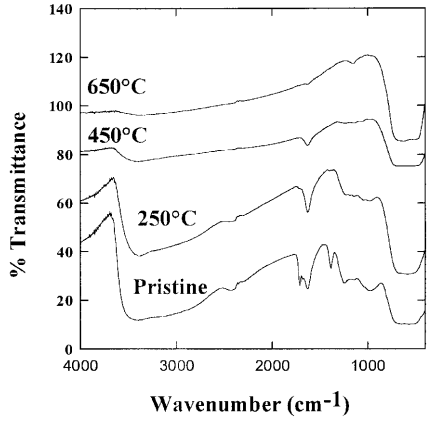

Fig. 6 FTIR spectra of pristine chemically decomposed tin oxalate and heat-treated products

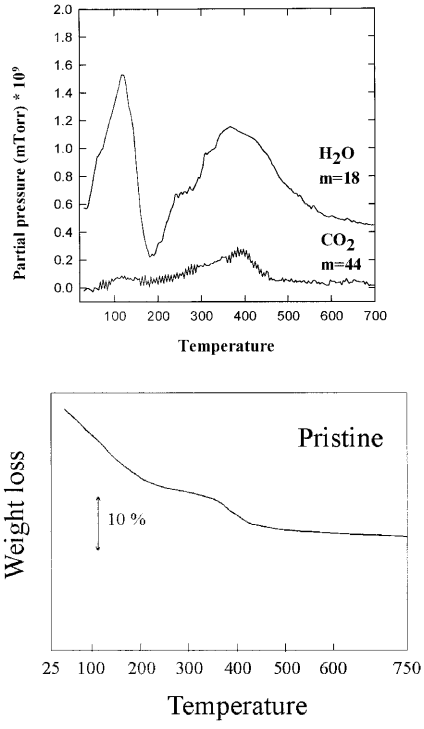

Fig. 7 EGA and TGA curves of chemically decomposed tin oxalate

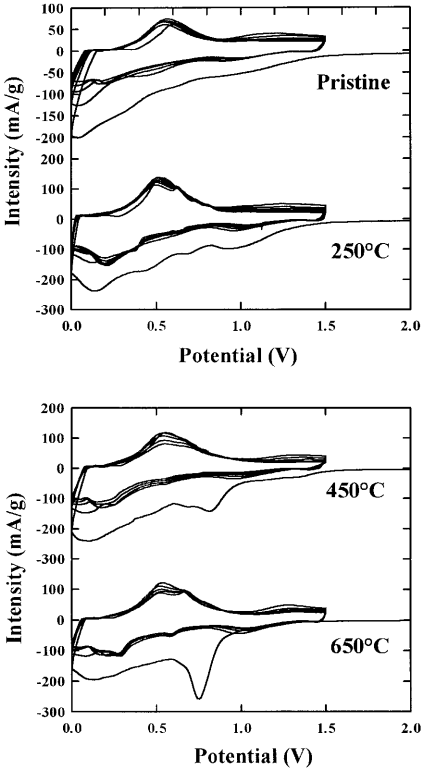

Fig. 8 Current intensity vs. potential curves obtained by SPES of lithium cells using SnO_2 from chemical decomposition of tin oxalate with H_2O_2 followed by heat treatment at 250, 450 and 650 °C

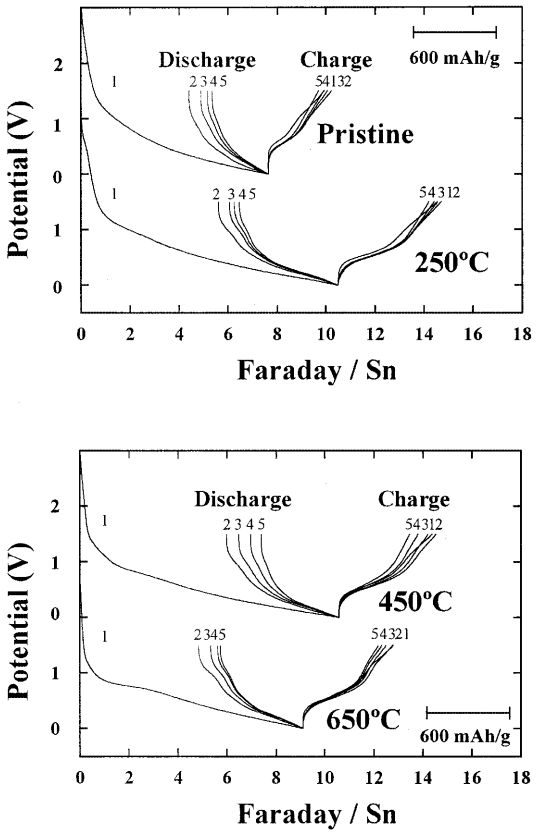

Fig. 9 Potential vs. composition curves obtained by SPES of lithium cells using SnO_2 from chemical decomposition of tin oxalate with H_2O_2 followed by heat treatment at 250, 450 and 650°C

On the other hand, Fig. 9 shows the potential/capacity plots for the first five cycles. The first discharge reaches the lowest values for the pristine sample (ca. 7.6 F/Sn or 1362 mAh/g), and the capacity retention is also poor. Both effects may be a consequence of the low electrical connectivity between particles as a result of the presence of surface adsorbed water. Globally, the thermally treated samples show higher capacities and better capacity retention (Fig. 9). The capacity of the first cell discharge ranges from 10.5 F/Sn (1867 mAh/g) for 250 °C treated samples to 9.2 F/Sn (1632 mAh/g) for 650 °C. These values are higher than expected for tin dioxide reduction (4 F/Sn) plus alloy formation (4.4 F/Sn). The discrepancy can be explained by the irreversible reaction of lithium with structural water which is lost below 600 °C. Finally, the best reversible capacity for the first cycle was obtained for the sample prepared at 250 °C (ca. 860 mAh/g). These results probably show the good influence of a homogeneous distribution of the structural water close to tin atoms all over the bulk particles prior to reaction with lithium, resulting in highly dispersed nanocrystalline Sn alloys, which can be considered a valuable factor for cycling. The best capacity retention (Fig. 9) was also achieved for a sample heat treated to 250 °C.

Conclusion

Tin oxalate is a potential candidate for electrode materials in lithium-ion batteries, as well as an interesting precursor for tin dioxide by both thermal and chemical procedures. The use of the pristine oxalate allows the formation of a dispersion matrix with a composition different from that obtained by starting with vitreous or crystalline tin oxides. The material is then appropriate to retain substantial capacity by a lithium-tin alloying mechanism, inhibiting the aggregation of tin domains. However, the cycling behaviour clearly falls below that found in other recently reported materials, such as the transition metal monoxides reported by Tarascon group [22] with 700 mAh/g capacities and excellent capacity retention during 100 cycles. A contribution to such a difference is the fact that lithium oxalate leads to irreversible reactions with lithium, while the formation and decomposition of Li_2O accompanying the reduction of metal particles was found to be highly reversible [22]. On the other hand, tin dioxide derived from tin oxalate by thermal and chemical treatments also shows good electrochemistry versus lithium. A procedure is proposed here to obtain ultrafine particles by oxidation of tin oxalate with aqueous hydrogen peroxide solutions. The resulting solid shows high surface and dispersion of the oxide and a significant content of surface and structural water, which is released in two steps. To avoid the major drawback resulting from surface reactions, a thermal treatment at 250 °C was found to optimize the cycling behaviour of these electrodes versus lithium.

Acknowledgements The authors acknowledge financial support from CICYT (contract MAT99-0741).

References

1. Schweizer-Berberich M, Strathmann S, Weimar U, Sharma R, Seube A, Peyre-Lavigne A, Göpel W (1999) Sens Actuators B 58:318
2. Manorama SV, Gopal Reddy CV, Rao VJ (1999) Nanostruct Mater 11:643
3. Mehrota RC (1990) J Non-Cryst Solids 121:1
4. Arai T (1960) J Phys Soc Jpn 15:916
5. Idota Y, Kubota T, Matsufuji A, Maekawa Y, Miyasaka T (1997) Science 276:1395
6. Courtney A, Dahn JR (1997) J Electrochem Soc 144:2045
7. Liu W, Huang X, Wang Z, Li H, Chen L (1997) J Electrochem Soc 145:59
8. Xiao YW, Lee JY, Yu AS, Liu ZL (1999) J Electrochem Soc 146:3623
9. Nagayama M, Morita T, Ikuta H, Wakihara M, Takano M, Kawasaki S (1998) Solid State Ionics 106:33
10. Fernandez Madrigal FJ, Perez Vicente C, Tirado JL (2000) J Electrochem Soc 147:1663
11. Brousse T, Retoux R, Herterich Schleich DM (1998) J Electrochem Soc 145:1
12. Retoux R, Brousse T, Schleich DM (1999) J Electrochem Soc 146:2472
13. Choy JH, Kim DH, Kwon CW, Hwang SJ, Kim YI (1999) J Power Sources 77:1

14. Zhecheva E, Stoyanova R, Gorova M, Alcantara R, Morales J, Tirado JL (1996) Chem Mater 8:1429
15. Alcántara R, Lavela P, Tirado JL, Stoyanova R, Kuzmanova E, Zhecheva E (1997) Chem Mater 9:2145
16. Nakamoto K (1986) Infrared and Raman spectra of inorganic and coordination compounds. Wiley, New York, p 232
17. Opara Krasovec U, Orel B, Hocevar S, Musevic I (1997) J Electrochem Soc 144:3398
18. Abello L, Bochu B, Gaskov A, Koudryavtseva S, Lucazeau G, Roumyantseva M (1998) J Solid State Chem 135:78
19. Li H, Huang X, Chen L (1999) J Power Sources 81–82:340
20. Aurbach D, Ein-Eli Y, Chusid O, Carmeli Y, Babai M, Yamin H (1994) J Electrochem Soc 141:603
21. Tunstall DP, Patou S, Liu RS, Kao YH (1999) Mater Res Bull 34:1513
22. Poitoz P, Laruelle S, Grugeon S, Dupont L, Tarascon JM (2000) Nature 407:496